# Gas Dynamic Effects On Laser Cut Quality

Kai Chen, Y. Lawrence Yao, and Vijay Modi
Department of Mechanical Engineering
Columbia University
New York, NY 10027

## Abstract

Cutting efficiency and quality are very sensitive to gas jet pressure and nozzle standoff distance. Do a high gas pressure and a small standoff distance necessarily give better material removal capability and cutting quality? Simple experiments to measure the mass flow rate were carried out for two types of geometry: a circular hole and a linear cut directly underneath an axisymmetric nozzle. The mass flow rate for the three dimensional case shows the same behavior (i.e., discontinuity as gas pressure and standoff change) as that of the axisymmetric case, indicating the basic shock structures of the axisymmetric case are applicable to the real cutting cases. The two important forces exerted by the gas jet for melt ejection, namely, shear force and pressure gradient are examined. Laser cutting experiments under the corresponding conditions were performed and the cut quality characterized by roughness, dross attachment, recast layer thickness was analyzed. The deterioration of cut quality is found to occur when the mass flow rate reaches bottom, which could occur at a high gas pressure or at a not so large standoff distance. It is thus indicative of the fact that the gas pressure and standoff distance affects cutting efficiency and quality through the underlying shock structure of the gas jet.

## Nomenclature

| | | | |
|---|---|---|---|
| $A_h$ | hole cross section area ($mm^2$) | $A_s$ | slot cross section area ($mm^2$) |
| $B$ | slot width (m) | $D$ | workpiece thickness (m) |
| $d$ | hole diameter (m) | $F$ | vector of x-directed fluxes |
| $H$ | nozzle standoff distance (m) | $L$ | slot length (m) |
| $m_h$ | through-hole mass flow rate (kg/sec) | $m_s$ | through-slot mass flow rate (kg/sec) |
| $p$ | static pressure (Pa) | $p_0$ | total pressure (Pa) |
| $p_t$ | total pressure (Pa) | $P_e$ | total pressure at delivery nozzle (Pa) |
| $r$ | radial coordinate (m) | $U$ | average velocity inside hole (m/s) |
| $x$ | axial coordinate (m) | $y$ | distance normal to the wall (m) |
| $\rho$ | density ($kg/m^3$) | $\tau$ | stress tensor |
| $\tau_{xr}$ | shear stress (Pa) | $\tau_{xx}$ | normal stress (Pa) |
| $\tau_{rr}$ | normal stress (Pa) | $\tau_a$ | average shear stress inside hole (Pa) |
| $\delta r$ | molten layer thickness (m) | $\delta p$ | pressure drop through hole |

## 1. Introduction

Assist gas plays an important role in laser cutting in order to eject melt from the cutting front. The cutting efficiency and cut quality are strongly dependent on the effective organization of the

gas jet. In industrial practice, convergent nozzles are commonly employed to direct a gas jet to the cut region of the workpiece. The operating pressure and the distance of the nozzle from the workpiece (standoff) are normally determined empirically in industrial practice. Pressure levels and large standoffs that deviate significantly can lead to poor and unrepeatable cut quality. A relatively high gas pressure and a relatively small standoff distance are considered to provide good material removal capability and thus good cut quality. Sometimes, poor quality is observed at a high-pressure level but the reasons are not necessarily clear. It is vaguely attributed to the complex nature of the shock structure associated with the supersonic gas jet impinging on a workpiece which can lead to unreliable behavior and poor cutting quality.

There are a number of experimental and theoretical investigations on the effects of the gas jet in laser cutting. Most of these research efforts have focused on the study of nozzle designs. The performance of various supersonic nozzles was studied by Larocca, et al. [1]. The off-axis configuration in tandem with a coaxial one was investigated by Chrysolouris and Choi [2], and the use of a single off-axis nozzle was studied experimentally by Brandt and Settles [3]. Less work has been performed to study the gas jet effects from the viewpoint of shock structure. The phenomena of the gas jet interacting with the cut kerf and the associated shock structures were studied by Makshev, *et al*. [4] and by Brandt and Settles [3] through experiments involving scale models. An analytical analysis of gas dynamic in laser cutting/grooving was given by Farooq and Kar [5]. A comprehensive review of the gas jet effects on laser cutting was presented by Fieret, *et al*. [6].

The study of the interactions between the gas jet and workpiece is of both theoretical and practical interests. Gas jets impinging on plates have been well studied but gas jets impinging on plates with certain features such as holes or slots have not been studied in detail. Practically, such study will enable the systematic determination of the optimal operation conditions so as to obtain high cutting efficiency and good cut quality. Prior to this study, an axisymmetric case, that is, a gas jet impinging on a workpiece with a concentric through hole, was studied (Chen, Yao, and Modi [7]). The melt was not considered based on the observation that it has little effect on the jet characteristic upstream of the workpiece. Measurement of the through-hole mass flow rate revealed the complex fluid flow phenomena, which were attributed to the shock structure change that were numerically determined in the same study but no cutting experimental results were presented.

The aforementioned study is extended in this paper to a non-axisymmetric case and supporting experimental evidence is obtained by cutting experiments. Measurements are taken for the mass flow rate through a slot rather than a concentric hole on the workpiece as in the earlier study. In addition, it is shown that shear force and pressure gradient, the two forces that eject the melt from the cut kerf exhibit a similar behavior as the mass flow rate. This clearly links the shock structure change to cutting efficiency and quality, which is verified in actual cutting experiments.

## 2. Numerical and Experimental Investigation of Axisymmetric Case

The current study is largely a continuation of the axisymmetric work by the same authors (Chen, Yao and Modi, [7]) plus cutting experiments. Most of the experimental and computational conditions of the present study parallel those of the previous study. Computer simulation was carried out for the calculation domain shown in Fig. 1. A simple experiment to measure the mass flow rate through the hole was designed to validate the simulation results. A collection box (also shown in Fig. 1) was placed directly underneath the workpiece to collect the flow and direct it to a measurement nozzle with a hole diameter much larger that the hole in workpiece. The gas velocity leaving the measurement nozzle is thus considerably reduced permitting accurate measurement by a hot-film velocimeter.

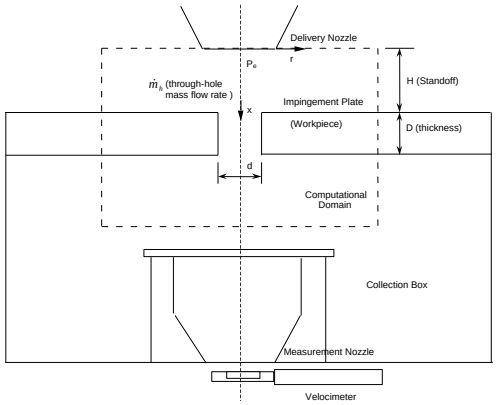


Fig. 1 Schematic of computational domain and experimental setup

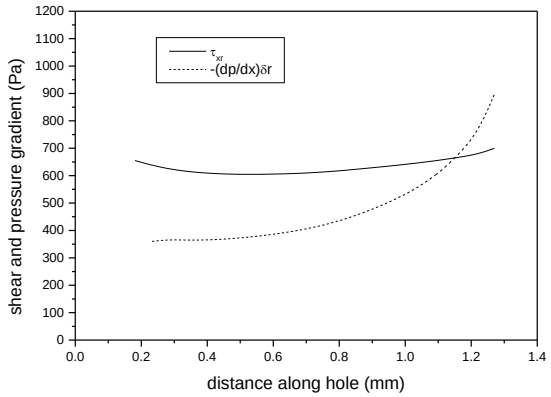


Fig. 2 Shear force and pressure gradient effects inside hole ($P_e$=363kPa, $H$=1.5mm, $d$=0.508mm)

In this paper, the axisymmetric case of a gas jet impinging on a workpiece with a concentric hole is further studied based on the shock structures revealed by the previous study. Material removal during laser cutting takes place by the ejection of molten material due to differential pressure and shear friction. If the molten material is not efficiently ejected, the cut surface quality will deteriorate. It is thus very important to evaluate the shear force and pressure gradient inside the hole.

The shear force and the pressure gradient are both related with the through-hole mass flow rate. The flow behavior inside the hole can be considered to be similar to that of a turbulent pipe flow because the thickness of the material is much larger than the hole diameter. For a turbulent pipe flow with a given geometry, both $\tau_{xr}$ (shear) and $\delta p$ (pressure drop) are proportional to $U^{7/4}$, where $U$ is the average velocity inside the hole. The through-hole mass flow rate is proportional to the average velocity:

$$m_h \propto \rho A_h U ,$$

where $\rho$ is the gas density and $A_h$ is the cross section area of the hole. Hence effects of both shear and pressure gradient are proportional to the through-hole mass flow rate. The effects of pressure gradient and shear stress can be approximately represented by

$$\frac{dp}{dx} D\pi d\delta r \text{ , and } \tau_{xr}\pi dD ,$$

where $d$ is the hole diameter, $D$ the workpiece thickness and $\delta r$ is the thickness of the shear boundary.

Fig. 2 shows typical shear force and pressure gradient effects inside the hole. The shear force and pressure gradient were calculated using the same solver as described in [7]. In comparing the effects of shear and pressure gradient, the shear layer $\delta r$ is taken to be the thickness of the molten layer and is assumed to be of the order of $10^{-5}$ m, which is commonly reported (Vicanek, *et al.*, 1986 [8]; Makashev, *et al.*, [4]). For convenience, we assume $\delta r = 2.0\times10^{-5}$ m and $D = 1.5$ mm. One then observes that the contributions of the shear force and the pressure gradient to the total force are of the same order.

Fig. 3 shows the effect of gas pressure on the variation of average shear force inside the hole ($\tau_a$) together with that of the through-hole mass flow rate. $\tau_a$ follows the same pattern as $m_h$ when $P_e$ varies. The maximum $\tau_a$ corresponds to the maximum $m_h$ and the minimum $\tau_a$ corresponds to the minimum $m_h$, which confirms that the change of shear force due to the change of shock structure can be reflected by the change of through-hole mass flow rate. The variation of $\tau_a$ and $m_h$ with standoff is shown in Fig. 4. Again, $\tau_a$ and $m_h$ exhibit a similar pattern as H varies while $P_e$ is fixed. We have explained the phenomena of a "bump" in $m_h$ with increasing $P_e$ while $H$ is fixed at 2 mm, and a "jump" in $m_h$ with increasing $H$ while $P_e$ is fixed at 363 kPa [7]. They are caused by the change of the shock structures either from direct interaction between the oblique shock and the normal shock to indirect interaction, or vice versa.

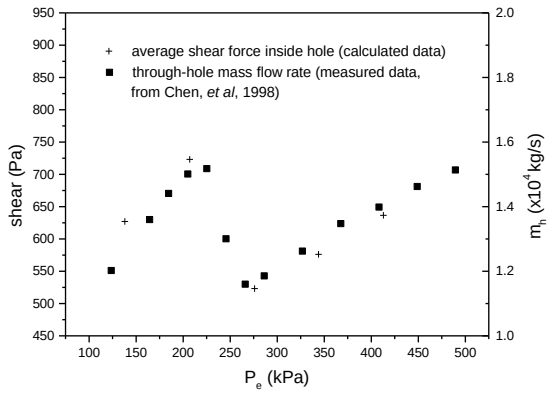


Fig. 3 Variation of average shear force inside hole and through-hole mass flow rate with total gas pressure (H = 2mm)

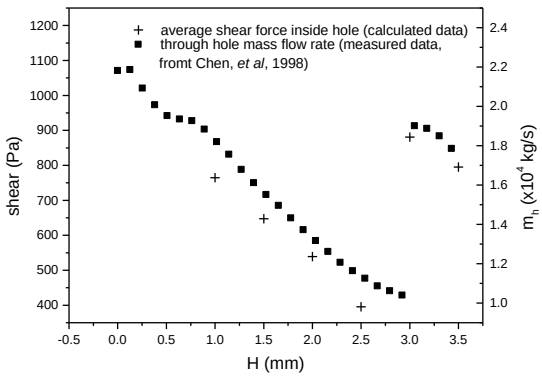


Fig. 4 Variation of average shear force inside hole and through-hole mass flow rate with standoff distance ($P_e$ = 363 kPa)

The axisymmetric study reveals that contributions of shear force and pressure gradient are of the same order of magnitude, and they follow the same profile as that of through-hole mass flow rate with the varying gas pressure and standoff. Several different hole sizes were tried in the calculation and the results reveal the same patterns of shear, pressure gradient and mass flow rate, indicating the hole size is not an important factor because its small scale compared to nozzle diameter.

## 3. Model Kerf Experiments

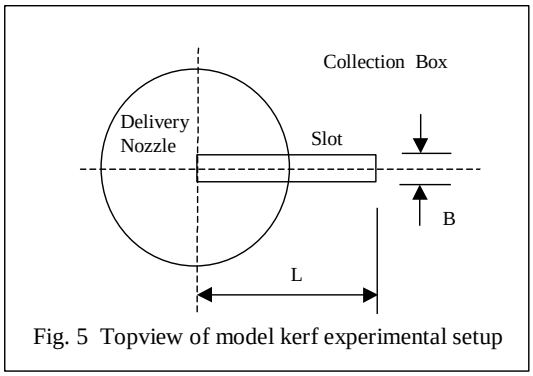

Fig. 5 Topview of model kerf experimental setup

In laser cutting, the gas jet interacts with the workpiece to generate a narrow cut kerf. The cut kerf geometry renders the problem three dimensional leading to departure from axisymmetric behavior. To examine this departure, experiments were carried out by replacing the hole on the workpiece with a slot that attempts to capture the essential geometric feature of the real cut kerf. The mass flow rate through the slot was measured using the collection box and measurement nozzle (Fig. 1). The impingement plate (workpiece) along with the collection box are placed on a precision x-y table so that one end of the slot end can be adjusted to align with the delivery nozzle axis (Fig. 5). The slot width (*B*) is set to be 0.22 mm, which equals the average kerf width in the subsequent real cutting experiments. It should be noted that the ability of a collection box to function requires that the pressure drop for the flow through the collection box is negligible compared to the pressure drop through the kerf. Thus, as the slot length increases and the pressure drop through the kerf decreases, a point is reached where the collection box resistance may no longer be negligible, allowing gas flow entering the slot to begin to reemerge. It is important to establish that the model kerf geometry does not reach such a point. In the experiments, the slot length *L* was maintained at 1.1 mm to ensure accuracy in measurement, while at the same time L is five times larger than *B* ensuring that the effect of the slot mimics a real cut kerf.

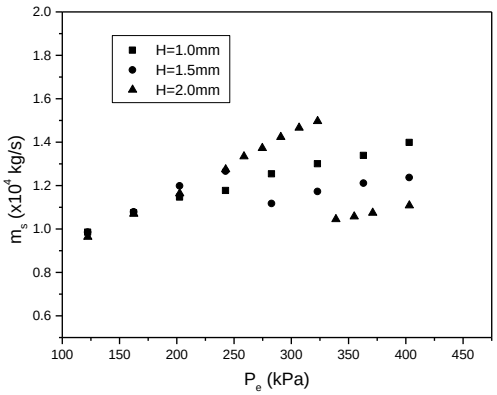

Fig. 6 Variation of through-slot mass flow rate with total gas pressure for *L = 1.1* mm

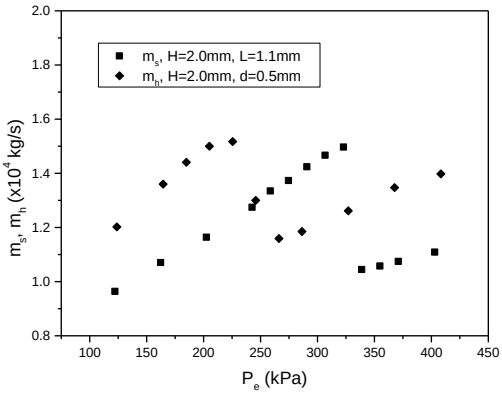

Fig. 7 Comparison of slot and through-hole mass flow rate for *H = 2.0* mm ($A_s \approx A_h$)

Fig. 6 shows the effect of gas pressure on through-slot (*L = 1.1* mm) mass flow rate $m_s$ for standoff distances *H = 1.0*, *1.5* and *2.0* mm. For *H = 1.0* mm, $m_s$ is found monotonically and linearly increase with $P_e$. For H = 2.0 mm, however, $m_s$ first increases with total pressure until it reaches a local maximum at $P_e$ = *325* kPa and then reduces even as total gas pressure increases, until it reaches a local minimum and begins to increase again. For *H = 1.5* mm, $m_s$ behavior lies in-between those of *H = 1.0* mm and *2.0* mm, and the local maximum and minimum are not evident. These phenomena are similar to those of $m_h$ behavior in the axsymmetric case. The "bump" in $m_s$ with varying $P_e$ for *H = 2.0* mm is caused by the change of shock structure as explained in Section 2.

If we compare the behavior of $m_s$ ($H = 2.0$ mm and $L = 1.1$ mm) and the behavior of $m_h$ ($H = 2.0$ mm and $d = 0.5$ mm) of two cases with the same cross-section area, we see that they resemble each other except that the "bump" shifts to higher $P_e$ values (Fig. 7). This is probably due to the fact that an edge of the slot is positioned at the center of nozzle (Fig. 5), causing less gas to enter the slot in comparison with the case of a concentric hole under the same pressure. The behavior of $m_s$ ($L = 1.1$ mm) with varying standoff is shown in Fig. 8 for nozzle pressure $P_e = 125, 243$ and 363 kPa. At $P_e$ values of 125 and 243 kPa, $m_s$ is relatively unaltered with increasing $H$. For $P_e = 363$ kPa, $m_s$ reduces continuously as $H$ increases then suddenly jumps to a high value at a critical standoff. Again these phenomena are consistent with those of an axsymmetric case.

Fig. 9 shows the comparison of the through-slot mass flow rate for $L = 1.1$ mm with the through-hole mass flow rate for $d = 0.5$ mm, both for a $P_e = 363$ kPa. Once again, the variations of $m_s$ and $m_h$ with varying standoff are very similar. They both show a sudden "jump" at about $H = 3.0$ mm. The fact that the $m_h$ value is larger than $m_s$ value for the same $H$ value is due to more gas entering the hole than entering the slot as explained earlier.

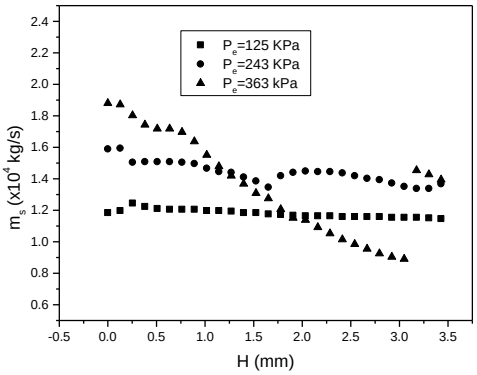


Fig. 8 Variation of through-slot mass flow rate with standoff distance for L = 1.1mm

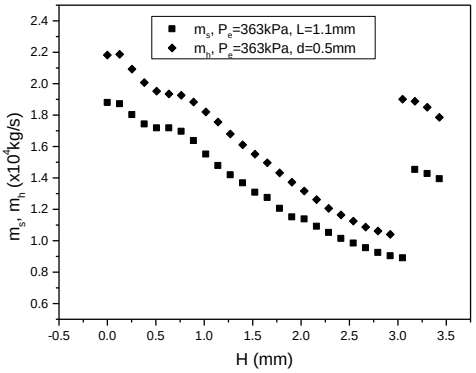


Fig. 9 Comparison of slot and through-hole mass flow rate for H = 2.0mm ($A_s \approx A_h$)

The overall trends in both through-slot and through-hole mass flow rate with varying gas pressure and standoff are the same. This implies that the gas jet interaction with a slot-type cut kerf has a similar shock structure to that of a concentric hole. Since the cut kerf width is considerably small as compared with the exit diameter of the delivery nozzle, the kerf geometry has little influence on the shock structure upstream of the workpiece. It is reasonable to expect the variation of the cut quality with varying gas pressure and standoff follows the same pattern of the variation of the through-slot mass flow rate. This is verified in the following section.

## 4. Laser Cutting Results and Discussion

To verify the gas jet effects on laser cut quality, laser-cutting experiments were carried out under the same conditions as those of the model kerf experiments. A PRC-1500 $CO_2$ laser with maximum output 1.5kW, operated in CW and $TEM_{00}$ modes was used for cutting experiments. The material being cut was cold-rolled mild steel of 1.6 mm thickness which has the same

thickness as the impingement plate in the through-hole and model kerf experiments for mass flow rate studies. In Group-1 experiments, air was used as assist gas for cutting, the gas pressure, $P_e$ was fixed at 363 kPa and the nozzle standoff distance, H was varied. In Group-2 experiments, oxygen was used for cutting, H was fixed at 2.0 mm and $P_e$ was varied from 122 kPa to 443 kPa which is the typical pressure range for oxygen assisted cutting of mild steels. Each group consisted of two experimental runs under the same conditions. These operating conditions given by gas pressure and standoff are identical to the conditions under which the through-slot and through-kerf mass flow rates were measured. To show their effects on cut quality most distinctively, the laser power and cutting speed were adjusted so that some samples were either barely cut through or not through at all. The laser cutting parameters for Group-1 and Group-2 experiments are listed in the following table:

| | Assist Gas | Gas Pressure | Standoff | Laser Power | Cut Speed |
|---|---|---|---|---|---|
| Group 1 | Air | 363 kPa | Varied | 800 W | 35 mm/s |
| Group 2 | Oxygen | Varied | 2.0 mm | 200 W | 40 mm/s |

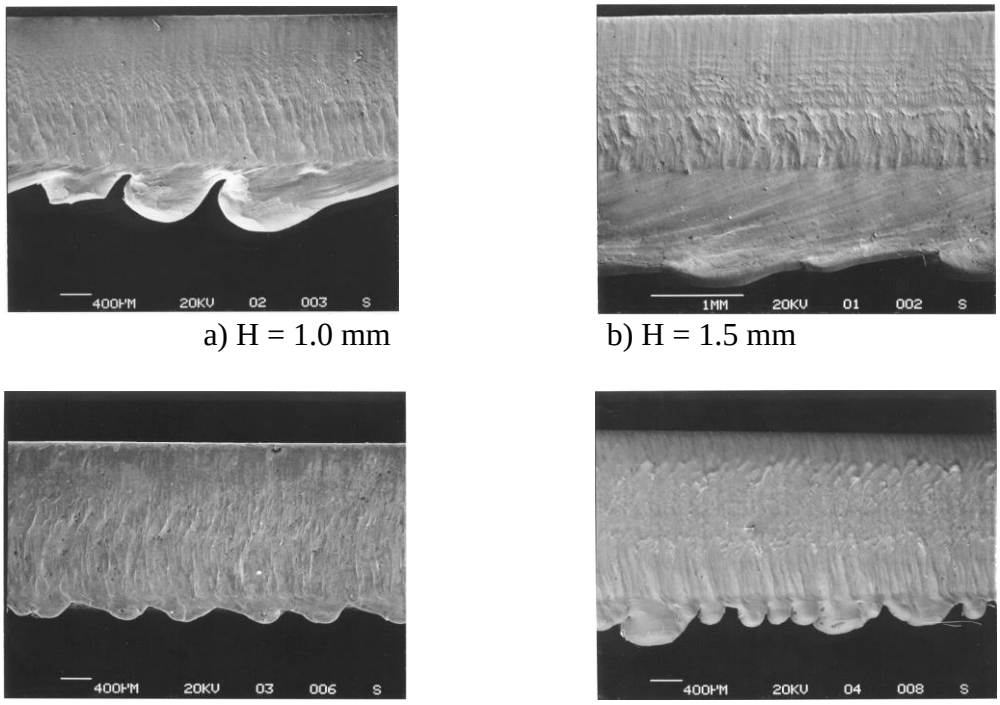


a) H = 1.0 mm b) H = 1.5 mm

c) H = 3.0 mm d) H =3.5 mm

Fig. 10 SEM of dross attachment on cut surface with different standoff at $P_e$ = 363 kPa (incomplete cuts for H = 2.0 and 2.5mm)

In Group-1 experiments, the less oxidized iron in the air assisted cutting has much higher viscosity and surface tension than the oxide-rich melt in oxygen assisted cutting (Ivarson, *et al*., [9]), and hence it is harder to eject the melt. Depending on the removal capability of the gas jet, resolidified melt (dross) may cling to the bottom edge of the cut kerf. It is expected that more dross will be attached to the edge, when the ejecting force exerted by the gas jet is weak, and vice versa. Fig.10 shows the dross attachment on cut edge with 4 different standoffs in the first run of

the experiments. Dross was observed at H = 1.0 mm. The amount of dross increases for H = 1.5 mm. Cuts were incomplete at H = 2.0 and 2.5 mm which is equivalent to extremely severe dross attachment. The dross attachment then suddenly decreases to a minimum amount at H = 3.0 mm, and it increases slightly at H = 3.5 mm. If the variation of dross attachment with standoff is compared with the variation of through-slot mass flow rate, it is seen that they exhibit opposite patterns. The sudden decrease in the dross corresponds to the jump of the through-hole mass flow rate. It is easy to understand this correspondence because the through-kerf mass flow rate has similar trends as the shear stress and pressure gradient, the two forces responsible for melt removal. So this study fundamentally explains why the total gas pressure and standoff have direct impact on the cut quality.

Each cut kerf in group-1 experiments was cross-sectioned and examined under SEM. Because of higher viscosity and surface tension associated with unoxidized molten iron, it is normally not all ejected from the cut zone in such inert-gas assisted cutting. The melt not ejected from the cut zone will resolidify on the cut surface and form a recast layer. The thickness of the recast layer varies depending on the removal capability of the gas jet, the larger the removal capability, the thinner the recast layer, and vice versa. Fig. 11 shows SEM pictures of the recast layer on the surface of the cut kerf of each sample from the second run. The recast layer increases as H increases from 1.0 to 1.5 mm, and then

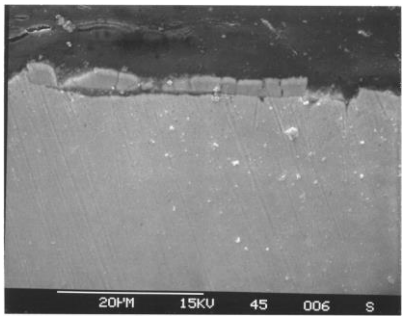


a) H = 1.0 mm

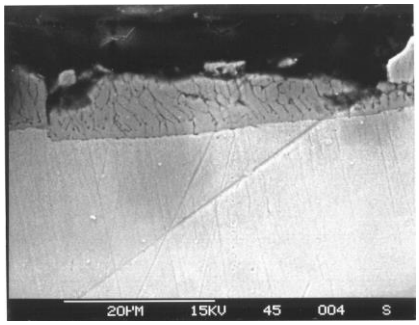


b) H = 1.5 mm

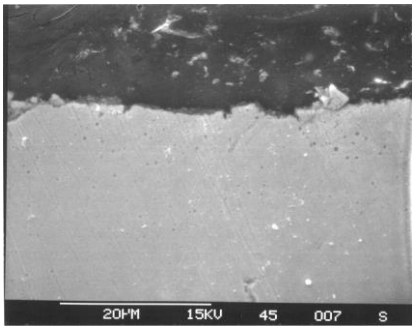


c) H = 3.0 mm

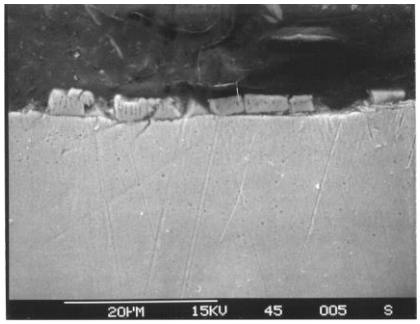


d) H =3.5 mm

Fig. 11 SEM of recast layer on cut surface with different standoff at $P_e$ = 363 kPa (incomplete cuts for H = 2.0 and 2.5mm)

decreases to a minimum value at H = 3.0 mm and again increasing slightly at H = 3.5 mm. If the cases of incomplete cuts at H = 2.0 and 2.5 mm are considered to be equivalent to the maximum recast layer, the pattern of change of the recast layer thickness with standoff is similar to that of dross attachment.

In Group-2 experiments, the samples were not cut through for $P_e$ = 323 kPa, 363 kPa in the first run, and for $P_e$ = 122 kPa, 363 kPa of the second run. SEM pictures of the cut kerf from the second run are shown in Fig. 12. On the upper portion of the cut kerf, regular stria are seen. Their formation involves more complicated physics and is studied by many researchers. On the lower portion of the cut kerf, there is a small amount of dross attached along the bottom edge, which indicates the melt is ejected from there. The surface finish of the lower portion is therefore more directly influenced by the ejecting forces of shear and pressure gradient associated with the gas jet. As seen, the surface finish at *Pe = 283* kPa is better that those at $P_e$ *= 162* kPa and $P_e$ *= 403* kPa. In fact, the best surface finish at the lower portion of the cut corresponds to a local maximum of the through-slot mass flow rate as indicated in Fig. 7.

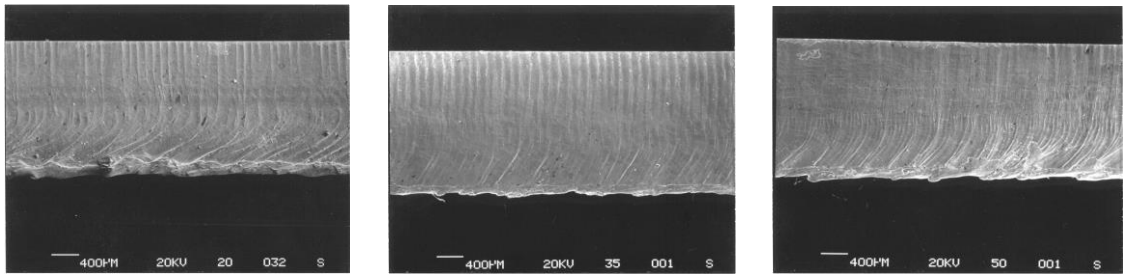


a) $P_e$ = 162 kPa b) $P_e$ = 283 kPa c) $P_e$ = 403 kPa

Fig. 12 SEM of cut surface with different gas pressure at 2.0mm standoff
(incomplete cuts at $P_e$ = 323 kPa, $P_e$ = 363 kPa)

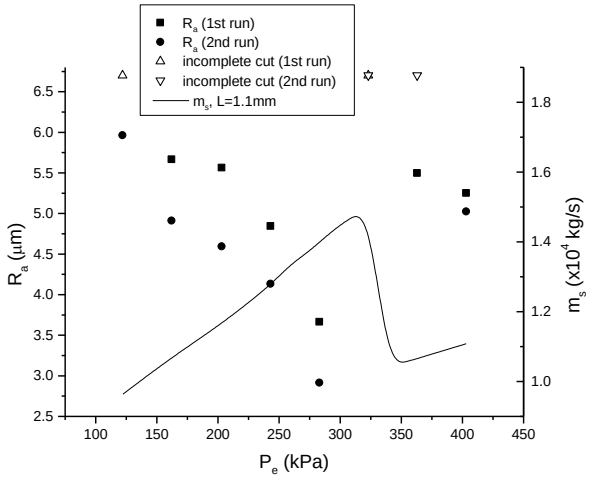


Fig. 13 Roughness ($R_a$) measurement at low portion of cut surface and through-slot mass flow rate measurement with different gas pressure at H = 2.0mm

Fig. 13 shows the roughness $R_a$ (root-mean-square average) of the lower portion of the cut vs. gas pressure at standoff $H = 2.0$ mm. It also shows the through-slot mass flow rate measurement. The situations where cuts are incomplete are marked with a triangle at the top of the figure to indicate they correspond to the maximum roughness. As seen, the roughness decreases as $P_e$ increases to about 300 kPa, before the cut becomes incomplete at $P_e = 323$ kPa, $R_a$ then decreases again as $P_e$ increases further. Comparing the variation of the roughness with the variation of the through-slot mass flow rate shown in the same figure, it is seen that the roughness follows a trend opposite to that of the through-slot mass flow rate. It is thus seen that a higher through-kerf mass flow rate corresponding to higher shear stress and pressure gradient results in better surface finish, whereas a lower through-kerf mass flow rate gives poor cut quality. The sudden drop of the mass flow rate with gas pressure for a standoff of $H = 2$ mm is due to the aforementioned change of the shock structures upstream of the workpiece.

The experimental results show that the cut quality including roughness, dross and recast layer vary with total gas pressure and standoff in a way strongly consistent with the pattern of change in the through-slot mass flow rate, which is in turn similar to that in the through-hole mass flow rate. The pattern of change in through-hole mass flow rate has been attributed to the changes in shock structure as evidenced in the axisymmetric simulation described in previous study [7]. This study shows that the primary behavior of shock structure in laser cutting is very similar to that in the axisymmetric case and it directly influences the cut quality.

## 5. Conclusions

The effects of a gas jet in laser cutting are examined. It is found that the removal capability of the gas jet, in terms of shear stress and pressure gradient, is affected by the shock structure of the impinging jet interacting with the workpiece. The through-hole or through-slot mass flow rate is found to be a key indicator of shock structure and removal capability of the gas jet. The variation of measured through-slot mass flow rate with gas pressure and standoff distance is similar to that of the through-hole mass flow (axisymmetric case), indicating that the basic shock structure of the two cases remains unchanged. Experimental measurement of cut quality characteristics such as roughness, dross attachment, recast layer thickness confirms their association with the shock structure and gas jet removal capability as predicted.

## Acknowledgement

This work is performed under the NSF grant DMI-9500181.

## References

[1] LaRocca, A. V., *et al*., *SPIE* 2207, 1994, pp. 169-180.
[2] Chryssolouris, G., and Choi, W. C., *SPIE Vol. 1042 $CO_2$ Lasers and Applications*, 1989, pp. 86-96.
[3] Brandt, A. D., and Settles, G. S., *J. of Laser Application*, Vol. 9, 1997, pp 269-277.
[4] Makashev, N. K., *et al*., *SPIE 2257*, 1994, pp. 2-9.
[5] Farooq, K., and Kar, A., *J. of Applied Physics*, Vol. 83, No. 12, 1998, pp. 7467-7473.
[6] Fieret, J., *et al.*, *SPIE Vol. 801 High Power Lasers*, 1987, pp. 243-250.

[7] Chen, K., Yao, Y. L., and Modi, V., Proc. ICALEO'98, Orlando FL, Laser Institute of America, 1998, Section B, pp. 120-129.
[8] Vicanek, M., *et al*., *J. Phys. D: Appl. Phys*., Vol. 20, 1986, pp.140-145.
[9] Ivarson, A., *et al*., *J. of Materials Processing Technology*, Vol. 40, 1994, pp. 359-374.